Acta Neuropathol (2015) 129:317–332
DOI 10.1007/s00401-014-1376-x

ORIGINAL PAPER

Traumatic brain injury-induced axonal phenotypes react differently to treatment

Anders Hånell · John E. Greer · Melissa J. McGinn · John T. Povlishock

Received: 2 November 2014 / Revised: 12 December 2014 / Accepted: 13 December 2014 / Published online: 21 December 2014

Abstract Injured axons with distinct morphologies have been found following mild traumatic brain injury (mTBI), although it is currently unclear whether they reflect varied responses to the injury or represent different stages of progressing pathology. This complicates evaluation of therapeutic interventions targeting axonal injury. To address this issue, we assessed axonal injury over time within a well-defined axonal population, while also evaluating mitochondrial permeability transition as a therapeutic target. We utilized mice expressing yellow fluorescent protein (YFP) in cortical neurons which were crossed with mice which lacked Cyclophilin D (CypD), a positive regulator of mitochondrial permeability transition pore opening. Their offspring were subjected to mTBI and the ensuing axonal injury was assessed using YFP expression and amyloid precursor protein (APP) immunohistochemistry, visualized by confocal and electron microscopy. YFP^+ axons initially developed a single, APP^+, focal swelling (proximal bulb) which progressed to axotomy. Disconnected axonal segments developed either a single bulb (distal bulb) or multiple bulbs (varicosities), which were APP^- and whose ultrastructure was consistent with ongoing Wallerian degeneration. CypD knock-out failed to reduce proximal bulb formation but decreased the number of distal bulbs and varicosities, as well as a population of small, APP^+, callosal bulbs not associated with YFP^+ axons. The observation that YFP^+ axons contain several pathological morphologies points to the complexity of traumatic axonal injury. The fact that CypD knock-out reduced some, but not all, subtypes highlights the need to appropriately characterize injured axons when evaluating potential neuroprotective strategies.

Keywords Traumatic brain injury · Axonal injury · Mitochondrial permeability transition pore · Cyclophilin D · Wallerian degeneration · Mouse

A. Hånell · J. E. Greer · M. J. McGinn · J. T. Povlishock (✉)
Department of Anatomy and Neurobiology, Medical College of Virginia Campus of Virginia Commonwealth University, Post Office Box 980709, Richmond, VA 23298-0709, USA
e-mail: jtpovlis@vcu.edu

Introduction

Over the last decade there has been considerable interest in traumatically induced diffuse axonal injury (DAI), which is recognized as an important underlying cause for the morbidity seen in patients following traumatic brain injury (TBI) [30, 38]. A better understanding of DAI has now emerged, primarily through postmortem histopathological studies and the use of advanced imaging performed in both the clinical and experimental settings [27, 29]. A particularly informative strategy has been the use of immunohistochemical labeling for amyloid precursor protein (APP), which accumulates at sites of impaired axonal transport [11]. The failure of the axonal transport system causes a gradual accumulation of both transported vesicles and organelles, which progresses to axonal swelling and axotomy.

In addition to the classical spheroid-shaped APP^+ swellings there are, however, reports of several other pathological axonal morphologies. These include multi-lobulated varicosities [22, 43], axons with an undulating trajectory [28, 43, 44], club-shaped disconnected axons [14, 42], and highly vacuolated swellings [41]. Unfortunately, it is currently unknown whether this heterogeneity is caused by the existence of different types of axonal injury, or if these diverse phenotypes represent different stages of a progressing pathology within the same axon. Gaining a better

understanding of these issues is important to enable a more detailed assessment of experimental therapeutics targeting axonal injury following TBI. In particular, it is crucial to distinguish between the events leading to axotomy and the ensuing downstream degeneration, since therapies targeting already disconnected axonal segments are unlikely to result in improved functional outcome.

To address these issues, we utilized mice that express yellow fluorescent protein (YFP) in a subset of neurons and evaluated them in a clinically relevant traumatic brain injury model. The fluorescent protein enabled an evaluation of the injury process in a distinct axonal population and a detailed study of the evolution of different pathological phenotypes over time. In addition to this morphological assessment we also attempted to modulate the axonal injury process, which has been purported to involve opening of the mitochondrial permeability transition pore (mPTP) with ensuing calcium dysregulation [11]. To evaluate this we utilized mice lacking the gene for Cyclophilin D (CypD), which is known to facilitate opening of the mPTP [3, 8, 20], a strategy which has proved successful in several pre-clinical disease models [15, 20, 37]. The unique properties of these mice thus allowed us to study not only the progression of injury within a well-defined axonal population, but also the effect of mitochondrial protection on the different pathological phenotypes occurring in these axons.

Materials and methods

Experimental animals

The mice used in this study were generated by crossing two existing mouse lines, one that expresses fluorescent protein in a subset of neurons and another that is genetically modified to inhibit opening of the mPTP. The first line expresses YFP under control of the Thy1-promoter (YFP-H) and was acquired from Jackson Labs [B6Cg-TgN(Thy1-YFP-H)2Jrs, stock number 003782; Bar Harbor, ME, USA] [19]. Inheritance of the YFP transgene was verified by inspecting ear punches using a fluorescence microscope (Olympus DP71, Olympus, Center Valley, PA, USA) as previously described [17].

The second line consisted of CypD knock-out mice generated as previously described [5]. This mouse line has been extensively characterized and the intra-mitochondrial Ca^{2+} concentration can reach levels almost twice as high in knock-outs, compared to wild types, before opening of the mPTP and the ensuing detrimental Ca^{2+} efflux [5, 20, 32]. CypD genotype was assessed using DNA extracted from tail clips with DNeasy Blood and Tissue Kit (Qiagen, Venlo, The Netherlands, cat nr 69504) and the *ppif* gene, which encodes CypD, was amplified by PCR using the forward primer GTA GAT GTC GTG CCA AAG ACT GCA G and the reverse primer AGC TGC AGG CCC TTG TCA CCA GTG CA. The DNA was then separated on a 1.5 % agarose gel which resulted in a clearly visible band at the expected size of approximately 560 bp in controls but not in knock-out mice.

The original lines were extensively backcrossed to a C57bl background by the original investigators before further breeding in our laboratory. The two lines were crossed followed by identification of YFP expressing $ppif^{-/-}$ mice, which were used for further breeding. Their offspring were used in the study and referred to as knock-out (KO). Mice from the original YFP-H strain were used as controls and are referred to as wild type (WT). All mice in the study were young adult males (mean age 10.0 weeks, range 8.0–11.4 weeks) with weights (mean 23.9 g, range 20.1–27.1 g) expected for this age group. The mice were group housed in a 12 h/12 h non-reversed light cycle on corn cob bedding with pressed cotton squares for nest construction and continuous free access to food and water.

Mild central fluid percussion injury and physiological monitoring

The cFPI procedure was performed according to previous descriptions [23], with the addition of physiological monitoring. General anesthesia was induced using 4 % isoflurane in oxygen and maintained at 2 % while core body temperature was kept at 37 °C using a feed-back controlled heating pad (Harvard Apparatus, Holliston, MA, USA). To verify that respiratory rate, arterial oxygen saturation and heart rate remained within physiological limits they were measured using a pulse oximeter (MouseOx; Starr Life Sciences, Oakmont, PA, USA) attached to the right thigh. The head was shaved followed by application of lidocaine gel and betadine/isopropyl alcohol. A midline incision was then made and a plastic trephine guide was attached, at the midline halfway between bregma and lambda using tissue adhesive (Vetbond, 3M, St. Paul, MN, USA) to enable the creation of a 3-mm craniotomy using manual trephination. A plastic hub was then placed over the craniotomy and temporarily attached using super glue gel and secured using dental acrylic. The animal was then allowed to recover for at least 1 h before being re-anesthetized and attached via the hub to a fluid percussion device (Custom Design and Fabrication; Virginia Commonwealth University; Richmond, VA, USA) followed by delivery of a 1.7 ± 0.04 atmospheres pressure pulse to the brain. Following injury the hub and dental cement were removed, the incision was sutured, lidocaine and bacitracin were applied and the time to recover the righting reflex was measured. All procedures described were approved by the Institutional Animal Care and Use Committee (IACUC) of Virginia Commonwealth University.

Perfusion and tissue sectioning

After survival periods of either 3 or 24 h the mice were anesthetized with an intraperitoneal injection of 1.6 mg/g sodium pentobarbital. When fully anesthetized, and unresponsive to toe pinch, the animals were transcardially perfused at 7 ml/min for 5 min with heparinized (10 U/ml) isotonic saline followed by either 4 % paraformaldehyde in phosphate buffer saline (PBS) for fluorescence microscopy, or by 4 % paraformaldehyde and 0.2 % glutaraldehyde in PBS for electron microscopy, for 10 min followed by post-fixation overnight. The brains were then coronally sectioned using a vibratome (Leica VT1000 S, Wetzlar, Germany) at 100 µm for fluorescence microscopy or at 40 µm for electron microscopy. Tissue sections were collected from bregma level −1.0 to −3.0 mm to span the region directly below the craniotomy, and then stored in 24-well plates in Millonig's buffer before being processed as indicated below.

Experimental design

All evaluations using fluorescence microscopy were performed using 24 mice divided into 6 groups based on injury status, *ppif* genotype and survival time. These groups were Sham-WT-24 h ($n = 2$), Sham-KO-24 h ($n = 2$), cFPI-WT-3 h ($n = 5$), cFPI-KO-3 h ($n = 5$), cFPI-WT-24 h ($n = 5$), cFPI-KO-24 h ($n = 5$). All quantitative assessments were performed blinded and surgical procedures for the different groups were intermingled to avoid systematic errors. Key findings from the quantitative fluorescence analysis were confirmed based on qualitative EM analysis using tissue from a separate cohort of mice detailed below.

Categorization and quantitation of YFP-positive damaged axons

The morphology and quantity of YFP^+ damaged axons in the experimental animals were determined using one section each from the bregma levels −1.6, −2.1 and −2.6 mm. Sections were selected by an investigator blinded to injury status, survival time as well as genotype and were then mounted on gelatin-coated slides, cover-slipped using Vectashield HardSet with DAPI (Vector Laboratories, H-1500) and analyzed in a blinded fashion. Since only a subset of axons are YFP^+ and only a fraction of all axons are damaged by mild cFPI, the intersection of the two sets was small and YFP-positive damaged axons tended to be few and spatially segregated. To enable a detailed evaluation at high magnification of this diffusely dispersed pathology a two-step approach was used. First the motorized stage and a 10× objective of a Zeiss LSM710 was used to acquire tiled images (2.6 × 7.7 mm) spanning the entire dorsal cortex and corpus callosum. These images were then imported into custom-written software which divided them into regions which could be sequentially viewed, one at a time, at high magnification. The software also made it possible to label and number damaged axons by mouse-clicking. The type of focal symmetrical increase in axon diameter typically seen following TBI, which we here term bulb, was reliably detected in these images but axonal segments connected to them could not be identified with confidence. In a second step, the labeled overview images were used as guides when performing a detailed evaluation of the damaged axons. This was done through the eye-piece of an LSM700 using a 40× objective, which allowed reliable detection of axonal segments connected to the bulbs identified in the previous step. The number of bulbs was counted in every damaged axon and for axons with two or more bulbs the presence of connecting axonal segments was also evaluated. Each damaged axon was also categorized as being localized in either the neocortex or the corpus callosum and the damaged axonal segment was assessed to determine if it was disconnected from the proximal and/or distal axonal segment. The distance to the edge of the corpus callosum from bulbs in damaged cortical axons was also measured using the labeled overview images with the aid of the custom-written software.

APP immunohistochemistry

Amyloid precursor protein is a widely used and well-recognized marker of axonal injury [11, 40] and we have previously reported that it labels some, but not all, YFP^+ bulbs [23, 24]. We used APP immunofluorescence to differentiate between subsets of YFP^+ axonal bulbs and to determine if there were categories of APP^+ axonal bulbs which never form in YFP^+ axons. APP labeling was performed using three free–floating sections from each animal taken from bregma levels adjacent to the ones used for the YFP quantification. The sections were blocked for 2 h in 10 % normal goat serum (NGS) and 0.5 % Triton X-100 in phosphate buffered saline (PBS) followed by an overnight incubation in blocking solution with the polyclonal rabbit primary antibody directed at the C-terminus of APP at 1:700 (Invitrogen, 51-2700, PAD CT695). The sections were then washed for 3 × 5 min in 1 % NGS and 0.2 % Triton X-100 in PBS and incubated with a secondary goat anti-rabbit Alexa Fluor-568 antibody (Molecular Probes, A1106) diluted 1:1,000 in the same solution, followed by an additional 3 × 5 min wash. After the final wash, the sections were mounted on gelatin-coated glass slides and cover-slipped using Vectashield HardSet with DAPI (Vector Laboratories, H-1500). Areas with intense YFP fluorescence devoid of APP labeling, and vice versa, were used to confirm absence of spectral bleed-through

between channels. Further, the negative controls (absence of primary antibody) were devoid of APP swellings. These controls provided confidence that the acquired images were representative of actual protein distribution.

Quantitation of YFP and APP co-localization

To evaluate the presence of YFP/APP double-positive bulbs the extent of co-localization was quantitated on a pixel-by-pixel basis. The images used were acquired bilaterally from the three immunoreacted sections from two regions in each hemisphere giving a total of 12 images from each animal. The first region was localized in Layer V of the neocortex while the other primarily encompassed the corpus callosum, but also parts of the deep cortex. Both regions were centered 1 mm from the midline in the medio-lateral direction. For brevity, the second region is hereafter referred to as the callosal region. The images were acquired as a single optical slice 1 µm thick, located in the center of z-plane of the section, using the 40× objective of a confocal microscope (LSM710, Zeiss, Jena, Germany) and each image consisted of three side-by-side sub-tiles which were digitally stitched together to make the final image cover an area of 626 × 216 µm. In areas where YFP and APP co-localize, a higher proportion of pixels with high intensities of both fluorophores should result. To measure this proportion, the number of pixels was counted for every possible combination of YFP and APP fluorescence intensity using custom-written Java software. The number of pixels was then used to create a heat map to visualize the frequency of pixels for every combination of fluorescence intensities. The colors used in the heat map were based on the color scheme Jet as defined in MatLab (version 8.3, MathWorks, Natick, MA, USA). Since only a subset of neurons express YFP and only a fraction of their axons are injured the number of pixels representing co-localized areas were expected to be low. As anticipated the number of low-intensity background pixels vastly outnumbered the high-intensity pixels, which made it difficult to visualize the extent of co-localization. To resolve this issue, a gamma adjustment ($\gamma = 0.1$) was applied to the pixel counts to emphasize low-frequency intensity combinations. The use of both the color scheme and the gamma adjustment did, however, introduce a non-linear relationship between pixel count and heat map color. Because of this the proportion of pixels with fluorescence intensities reliably indicating co-localization was also calculated and used as an objective quantitative measure of the extent of co-localization.

Quantitation of APP-labeled bulbs

The images used for the co-localization study were also used to quantify the number and size distribution of APP-labeled bulbs. The number of APP swellings and their sizes were automatically counted using ImageJ (version 1.46r, NIH, Bethesda, MA, USA) by first using the function 'Color Threshold' to set the brightness threshold to 50 followed by the function 'Analyze Particles' with a size threshold of 250 pixels [31]. The option 'Overlay masks' was used to visualize the bulbs detected by the automated method to verify that they corresponded to pathological APP accumulations.

Electron microscopy

Separate groups ($n = 3$ each) of both WT and KO mice were used for qualitative electron microscopic (EM) assessment of axonal injury at both 3 and 24 h post-injury. These animals were perfused and their brains sectioned as described above, followed by immunohistochemical labeling using antibodies to either YFP or APP. Multiple sections harvested near the same loci previously assessed via confocal analyses were first rinsed four times in phosphate buffered saline (PBS), endogenous peroxidase activity was quenched using 0.5 % H_2O_2 in PBS for 30 min followed by temperature-controlled microwave antigen retrieval [42]. After this the sections were pre-incubated for 1 h in 10 % NGS with 0.2 % Triton X-100 in PBS followed by overnight incubation in either a 1:7,500 dilution of a rabbit polyclonal anti-GFP antibody (AB3080, Milipore), which also recognizes YFP, or a rabbit polyclonal antibody directed against the C-terminus of APP at 1:2,500 (Invitrogen, 51-2700, PAD CT695). The sections were then incubated for 1 h in biotinylated goat-rabbit secondary antibody at 1:200 in a solution of an avidin-horseradish peroxidase complex (ABC Standard Elite Kit, Vector). The reaction product was visualized with 0.05 % 3,3′-diaminobenzidine (DAB), 0.01 % H_2O_2 and 0.3 % imidazole in 0.1 M phosphate buffer for 10–20 min. The tissue was then osmicated, dehydrated, and flat embedded between plastic slides in mid cast resin (Ted Pella, Redding, CA, USA). The embedded slides were then scanned to identify regions containing injured axons within Layer V and the corpus callosum. These were then removed and mounted on plastic studs followed by thick sectioning to a depth of the immunoreactive product of interest. Serial 70-nm sections were cut and picked up onto formvar-coated slotted grids followed by staining in 5 % uranyl acetate in 50 % methanol for 2 min and 0.5 % lead citrate for 1 min. Ultrastructural analysis was conducted using a JEM 1230 transmission electron microscope equipped with an Ultrascan 4000SP CCD camera.

Poisson distribution curve fitting

Axons with multiple bulbs were found in this material and the statistical distribution of the number of bulbs found within individual axons was evaluated. This type of data

(non-negative integers) often follows a Poisson distribution in biological samples [25], and the data was therefore fitted to this distribution. The shape of the Poisson distribution is determined by a single value (λ) which normally can be calculated by taking the mean value of the observations. Since axons with multiple bulbs by definition have at least two bulbs this method cannot be used in this case, and the λ-value was instead determined by using the least squares method to minimize the residuals. The fitted curve was then extrapolated to determine the expected number of this type of injured axons containing a single bulb.

Statistics

For group-wise comparisons, the data were first assessed for normality using Shapiro–Wilks (SW), and if the data in all groups were normally distributed they were analyzed using a one-way ANOVA, which if significant was followed by post hoc testing with a Tukey (TU) correction for multiple comparisons. Non-normal data were first analyzed using Kruskal–Wallis (KW), which if significant was followed by post hoc testing with Benjamini and Hochberg (BH) correction for multiple comparisons [7]. Data are presented as mean ± SEM and individual animals were considered to be the statistical unit. To better visualize the results the graphs display individual data points, when practically possible, rather than using bar graphs. Comparisons of statistical distribution were made using the two-sample Kolmogorov–Smirnov (KS) test.

Data entry was performed in Microsoft Excel 2010, statistical analysis made in R (version 3.03), graphs created using GraphPad Prism (version 5.04, GraphPad Software, La Jolla, CA, USA) and the final assembly of figures made in Adobe Illustrator CS6 (version 16.0.5, Adobe Systems, San Jose, CA, USA). Significance levels are designated as not significant (ns) for $p \geq 0.05$, * for $p < 0.05$, ** for $p < 0.01$ and *** for $p < 0.001$.

Results

Physiological monitoring

The results from the physiological monitoring prior to injury agreed with previous observations of mice under isoflurane anesthesia [12, 18] for the assessed variables arterial oxygen saturation (mean 98.1 %; SEM 0.15 % in WT; mean 98.4 %; SEM 0.15 % in KO), heart rate (mean 508 bpm; SEM 17.2 bpm in WT; mean 472 bpm; SEM 13.7 bpm in KO), and respiratory rate (mean 63.1 bpm; SEM 2.32 bpm in WT; mean 63.6 bpm; SEM 2.80 bpm in KO). CypD knock-out did not significantly affect any of the measured variables ($p > 0.1$ for all variables). Importantly, there were no episodes of hypoxia while the oxygen saturation remained above 95 % and the respiratory rate above 30 min^{-1} for more than 98 % of the monitored time in each animal. Core body temperature was not continuously recorded, but was checked frequently during surgery and found to be reliably maintained between 36.5 and 37.0 °C by the feed-back controlled heating pad.

Righting reflex recovery

The time to recover the righting reflex was measured to quantify the magnitude of the injury and was found to follow a non-normal distribution and differed significantly between groups (KW; $^{**}p = 0.007$). The time to recover the righting reflex was significantly (BH; $^{*}p = 0.045$) longer in brain-injured WT mice (mean 6.1 min; SEM 1.0 min) compared to sham-injured WT mice (mean 1.9 min; SEM 0.3 min) consistent with previous observations using this model [23, 24]. This was the case in the KO mice as well, with a significantly (BH; $^{*}p = 0.045$) longer reflex recovery time following brain injury (mean 7.5 min; SEM 0.8 min) compared to sham-injury (mean 1.1 min; SEM 0.2 min). There was, on the other hand, no significant difference (BH; ns $p = 0.076$) between brain-injured WT and KO mice, indicating that both groups sustained comparable levels of injury. The transient loss of the righting reflex in sham-injured animals was most likely related to the anesthesia and not an effect of the sham-injury procedure itself.

Morphology of YFP^+ axons following sham-injury

The brain tissue from both WT and KO mice appeared normal without any indication of hemorrhage or necrosis induced by the surgical procedures. Consistent with previous descriptions of these mice [19, 23, 24], the cortical YFP expression was located primarily in a subset of Layer V pyramidal neurons (Fig. 1a). Their axons could be traced from their cell bodies of origin in Layer V ventrally through the gray matter until they entered the corpus callosum and turned laterally to follow this fiber tract. The axons typically followed a relatively linear course but some axons in both white and gray matter followed a wavy, undulating, trajectory, termed undulations (Fig. 1). The presence of undulations in sham-injured animals suggests that this morphology is unrelated to mechanical trauma but potentially caused by tissue preparation. Neither WT nor KO sham-injured mice revealed any axonal bulbs or other abnormalities except for undulations.

Injury-induced YFP^+ axonal morphologies

Comparable to the sham-injured mice, the brain-injured mice did not display any signs of petechial hemorrhage

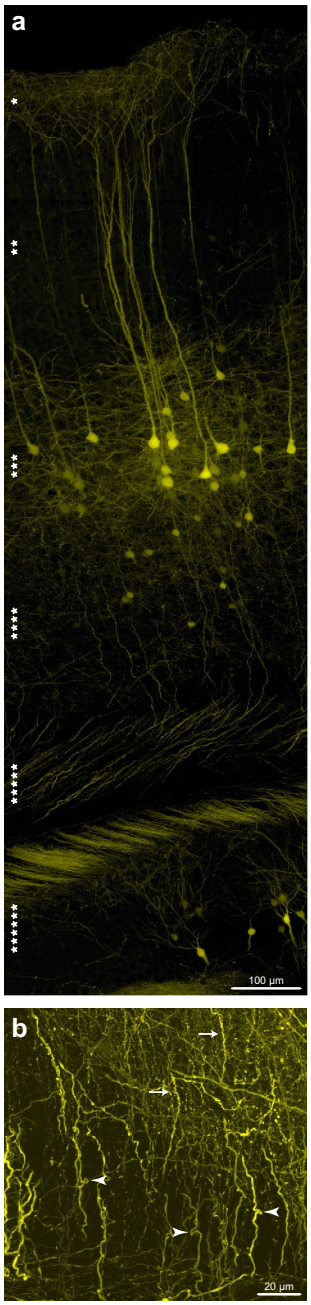

Fig. 1 YFP expression in sham-injured animals. **a** The majority of cortical cells expressing YFP were Layer V pyramidal neurons (***), which extend their dendrites (**) toward the cortical surface (*), and their axons ventrally through Layer VI (****) and into the corpus callosum (*****), but not the underlying hippocampal formation (******). Note that some axons within the corpus callosum have a wavy, undulating trajectory (undulations). **b** Undulating axons (*arrows*) and highly distorted axonal profiles (*arrowheads*) were found close the midline in Layer VI following sham-injury. These types of axonal trajectories were consistently found in sham-injured animals, indicating that they are unrelated to mechanical damage, but potentially induced by tissue processing

or cortical contusion, consistent with the mild and diffuse nature of this model, also detailed in our previous communications [23, 24]. In contrast to sham-injury the cFPI procedure induced the formation of axonal bulbs scattered throughout a region starting at cortical Layer V and extending ventrally towards, and including, the corpus callosum (Fig. 2a). Based on their morphology the majority of these axonal bulbs could be classified into three distinct populations.

The first population consisted of axonal bulbs disconnected from the distal axonal segment, yet remaining in continuity with the proximal segment (Fig. 2b, c). These were termed proximal bulbs and consistent with previous reports they typically had a diameter of 4–6 µm [23, 24]. The proximal bulbs were typically found close to, and in continuity with, their cell bodies of origin and based on results from previous communications [23], most likely localized to the axon initial segment (AIS) or para-AIS (Fig. 2c). Some proximal bulbs were also found in more ventral neocortical regions and could occasionally be traced back to their cell bodies of origin (Fig. 2b), although their axons were frequently found to leave the plane of the section before reaching the cell body.

Another category of axonal bulbs were disconnected from their proximal, but not distal axonal segments, and these were termed distal bulbs (Fig. 2d). Other injured axons were found to contain several bulbs in close proximity in a bead-on-a-string pattern, and were termed varicosities. The varicosities often contained only two bulbs (Fig. 2e), but were occasionally found to contain more than ten bulbs in close alignment (Fig. 2f), and individual bulbs within varicosities were typically connected with a thin axonal segment.

Together these three populations made up 481 of 517 evaluated injured axons (93 %), in WT mice and 236 of 256 (92 %), evaluated in KO mice, and any other, non-conforming, phenotypes were excluded from further analysis.

Temporal distribution of YFP^+ pathological morphologies

The number of proximal bulbs followed a normal distribution and there were significant (ANOVA; $^{**}p = 0.0021$) differences between the groups. The difference over time in WT animals was substantial, with an approximately threefold reduction in the number of proximal bulbs (TU; $^{*}p = 0.016$). CypD knock-out, on the other hand, did not have any significant effect on the number of proximal bulbs at either 3 or 24 h post-injury (Fig. 3a).

The temporal distributions of distal bulbs and varicosities were similar and in both cases followed a non-normal

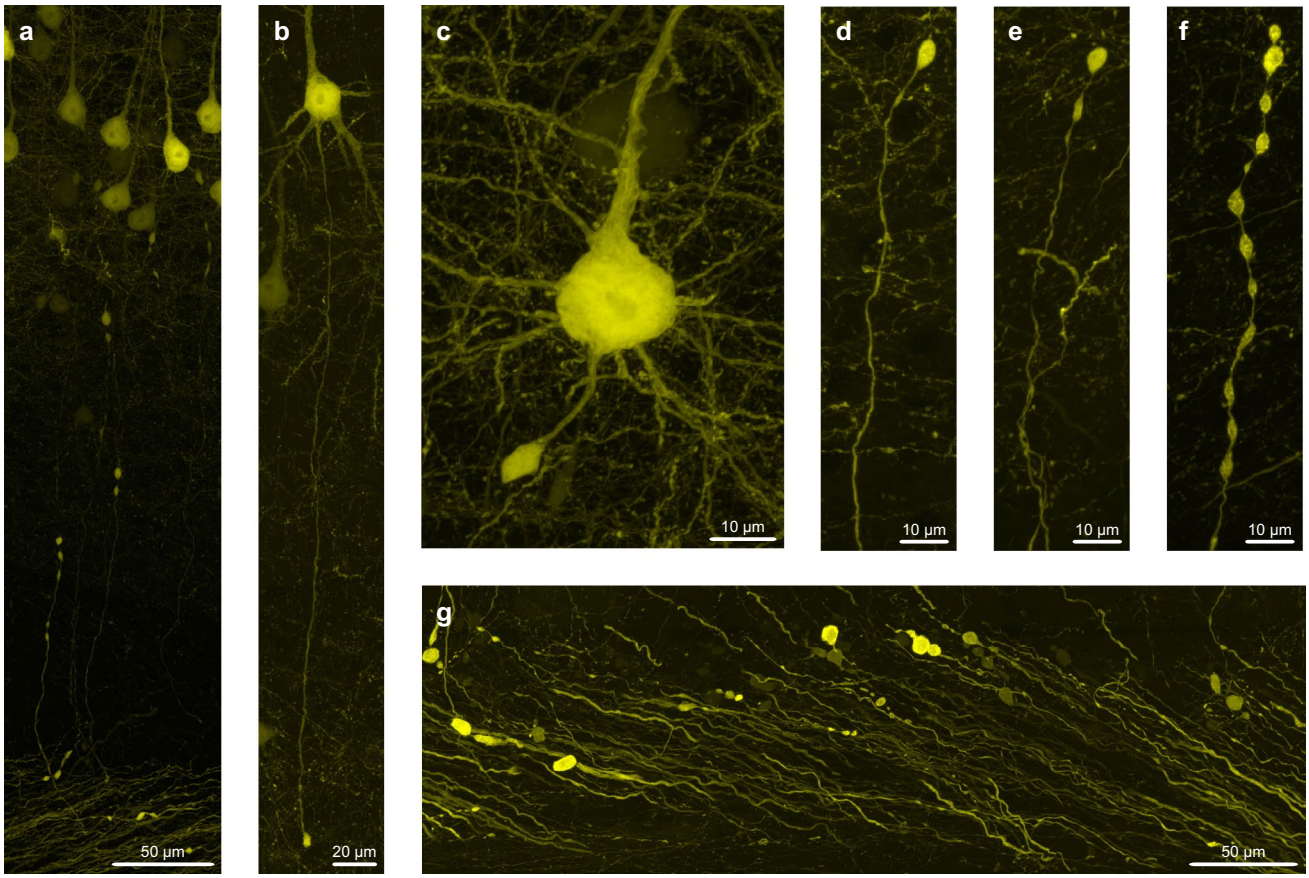

Fig. 2 Several pathological axonal morphologies were revealed by the YFP expression following cFPI. **a** Axonal bulbs were detected within the entire region from the cell bodies of the Layer V pyramidal neurons towards, and including, the corpus callosum. **b**, **c** Proximal bulbs were typically found at 3 h post-injury, sometimes located far from the cell body of origin (**b**), although typically within, or close to, the axon initial segment. **c** The proximal bulbs could typically, but not always, be traced back to their cell body of origin. **d** Distal bulbs were disconnected from their cell bodies of origin but still in continuity with the distal axonal segment. Varicosities with two bulbs (**e**) were the most common, but varicosities with up to twelve bulbs (**f**) were found. **g** The callosal region at 24 h post-injury was often found to contain numerous distal bulbs and varicosities, although, only rarely proximal bulbs

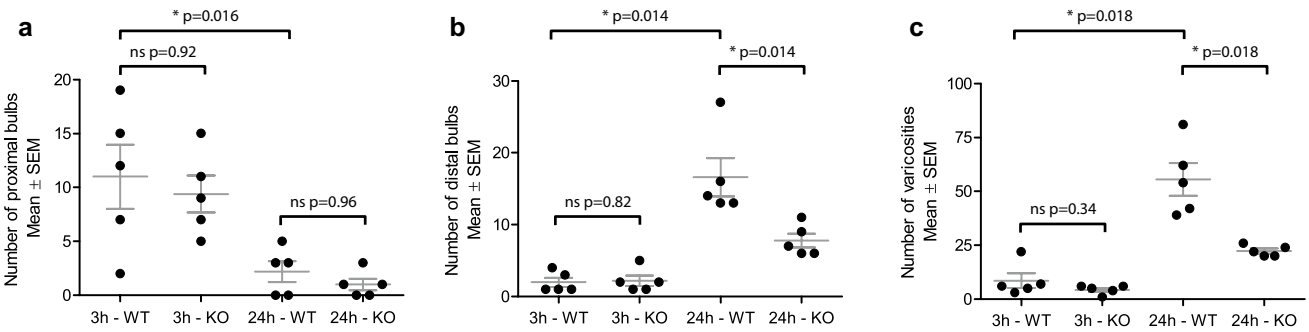

Fig. 3 Following injury the proximal bulbs predominate at early time points while distal bulbs and varicosities predominate at later time points. Each data point represents the number of each type of pathological morphology found in one animal. The number of proximal bulbs (**a**) decreases with time while distal bulbs (**b**) and varicosities (**c**) increase with time. CypD knock-out did not significantly affect the number of proximal bulbs, but substantially and significantly reduced the number of both distal bulbs and varicosities at 24 h post-injury

distribution with significant differences between groups for both distal bulbs (KW; ***$p < 0.001$) and varicosities (KW; **$p = 0.0014$). In stark contrast to the proximal bulbs, there was an approximately sixfold significant increase in the numbers of both distal bulbs (BH; *$p = 0.014$) and varicosities (BH; *$p = 0.018$) over time. The effect of CypD knock-out also differed from the proximal bulbs, and there was an approximately twofold, statistically significant, reduction in both the number of distal bulbs (BH; *$p = 0.014$) and varicosities (BH; *$p = 0.018$) at 24 h post-injury (Fig. 3b, c).

These results indicate that brain injury initially gives rise to proximal bulbs and at later time points distal bulbs and varicosities. It is also noteworthy that the results are also similar for distal bulbs and varicosities, while the results for the proximal bulbs diverge from the two other phenotypes.

Spatial distribution of YFP$^+$ pathological morphologies

To assess the spatial distribution all injured axons were classified as being either cortical or callosal. This revealed that proximal bulbs were almost exclusively cortical, and only 2 of 66 in WT mice, and 2 of 52 in KO mice, were located in the corpus callosum. The distal bulbs and varicosities, on the other hand, were frequently located in the callosal region, and the callosal fraction of both distal bulbs and varicosities increased over time (Fig. 4a).

To obtain a more detailed description of the spatial distribution the distance to the corpus callosum was measured for all injured axons in the cortex. This distance followed a normal distribution at both 3 and 24 h post-injury in WT mice differed between types of bulbs at both time points (ANOVA; ***$p < 0.001$ at 3 h; ANOVA; **$p = 0.0019$ at 24 h). In the KO mice the distance from the corpus callosum followed a normal distribution at 24 h, but not 3 h, post-injury, and differed significantly between the types of bulbs (KW; *$p = 0.011$ at 3 h; ANOVA; *$p = 0.022$ at 24 h). Consistent with frequent observations of both distal bulbs and varicosities within the corpus callosum the ones found in the cortex were typically located close to the corpus callosum. The proximal bulbs, on the other hand, were typically located at significantly longer distances from the corpus callosum compared to the distal bulbs and varicosities (Fig. 4b).

These data demonstrate that the proximal bulbs are located close to their cell bodies of origin while the distal bulbs and varicosities occur in more distal regions.

Characteristics of YFP$^+$ varicosities

The individual bulbs that comprised the varicosities were typically (92 % in WT mice; 94 % in KO mice) connected to each other by a thin axonal process (Fig. 2f). Varicosities

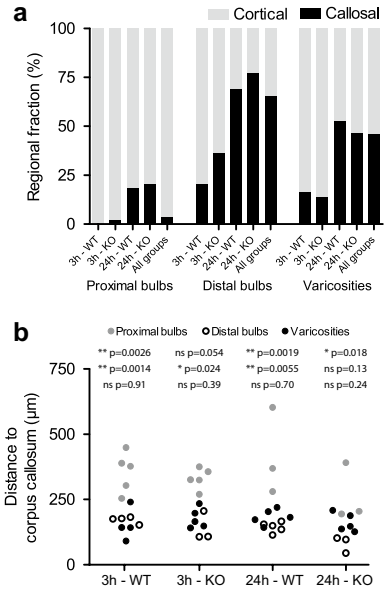

Fig. 4 Proximal bulbs typically reside close to their cell bodies of origin, in stark contrast to the location of distal bulbs and varicosities. **a** Distribution of swellings between the cortex and the corpus callosum. Note that proximal bulbs are almost exclusively found in the cortex while distal bulbs and varicosities are found in both regions. The fraction of injured axons found in the corpus callosum relative to the cortex also increases between 3 and 24 h post-injury, indicating that the pathology shifts to more distal regions over time. **b** Distance from the corpus callosum for all injured axons within the cortex, each data point represents the mean for one animal. The *top row* of *p* values refer to proximal bulbs versus distal bulbs, the *middle row* to proximal bulbs versus varicosities and the *lower row* to distal bulbs versus varicosities

were also typically (85 % in WT mice; 94 % in KO mice) connected to the distal axonal segment, but seldom (18 % in WT mice; 21 % in KO mice) to the proximal axonal segment. Due to the methodological issues associated with tracing individual axons for long distances attempts to assess if varicosities were in contact with their cell body of origin were not made. Varicosities were often located several hundred µm from their cell bodies of origin which implies that those connected to a proximal axonal segment were not necessarily in continuity with their cell bodies of origin.

To determine if either proximal bulbs or distal bulbs could be considered to be varicosities with a single bulb the statistical distribution of varicosities with different number of bulbs was examined. Varicosities with two bulbs were the most common and varicosities containing more bulbs were seen at progressively decreasing frequencies in both WT and KO mice. This data were found to fit well with a Poisson distribution, which is common for count data (non-negative integers) from biological samples [25]. This distribution was found to yield accurate predictions of the number of distal bulbs, but resulted in poor predictions of the

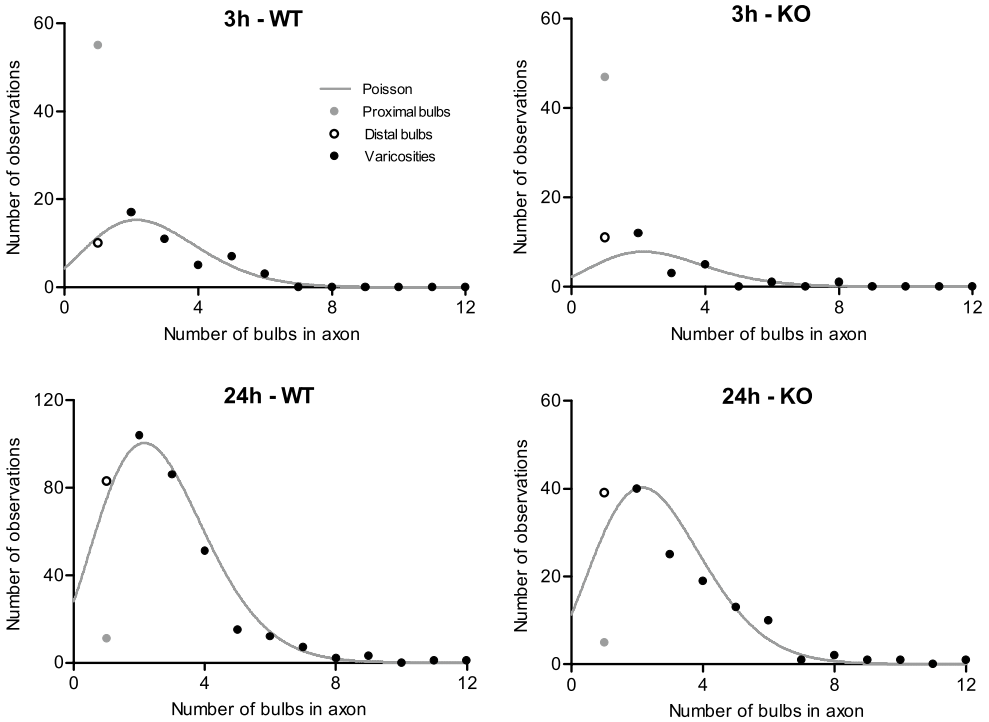

Fig. 5 The number of distal bulbs and varicosities follow a Poisson distribution. Varicosities with two swellings were the most common and varicosities with more swellings were seen at progressively decreasing frequencies, yet varicosities containing as many as 12 swellings could be found. To determine the relationship between proximal bulbs, distal bulb and varicosities, the number of observation of these three categories were plotted together and a Poisson distribution was fitted to the varicosity data. This distribution could not be used to predict the number of proximal bulbs, although it provided good predictions of the number of distal bulbs. This indicates a close relationship between distal bulbs and varicosities, which is not shared by the proximal bulbs

number of proximal bulbs, regardless of post-injury time point or genotype (Fig. 5).

This result supports the hypothesis that distal bulbs can be considered to be varicosities with a single bulb, which is further supported by the similarity observed in both spatio-temporal distribution and response to CypD knock-out.

Qualitative description of APP^+ pathology

Immunolabeling for APP was used to further characterize the axonal bulbs as it is a well-accepted marker for pathology in the axonal segment proximal to axotomy. At 3 h post-injury cortical Layer V contained multiple APP^+ axonal bulbs with a diameter of 4–6 µm (Fig. 6a), which were typically not found in other cortical and callosal areas. These bulbs were morphologically similar to the YFP^+ proximal bulbs and all proximal bulbs which could be clearly identified as being in continuity with their cell body were APP^+ (Fig. 6b, c). However, since only a subset of neurons expresses YFP, all large APP^+ axonal bulbs were not YFP^+.

Brain injury also induced the formation of a previously uncharacterized population of small APP^+ axonal bulbs, scattered throughout the cortex and the corpus callosum, which appeared quite numerous at both 3 and 24 h post-injury (Fig. 6d). Within the corpus callosum their diameters ranged from the threshold of reliable detection, at about 2 µm, up to, but seldom over, 4 µm. Although both these small APP^+ bulbs, as well as the YFP^+ distal bulbs and varicosities, were frequently found in the deep cortex and corpus callosum, especially at 24 h post-injury, no YFP^+APP^+ bulbs could be identified in these regions.

The morphology of the small APP^+ bulbs in both the cortical and callosal regions was comparable at 3 and 24 h post-injury while the morphology of the large APP^+ cortical bulbs changed substantially over time. At 3 h post-injury the large APP^+ accumulations typically had a round, almost spherical shape (Fig. 6c), but this morphology was rarely found at 24 h post-injury. Rather, at this time point it was common to find club-shaped APP^+ accumulations (Fig. 6e), as well as APP accumulations shaped like a bulb with an attached swollen axonal segment (Fig. 6f). Although rare, there were also axons in which APP accumulated in several adjacent bulbs connected to a swollen, APP^+, axonal segment (Fig. 6g). These multi-bulbous, APP^+ axons, were found in, or near, Layer V of the cortex and were unrelated to the YFP^+ varicosities, which did not label with APP and were typically located in deep cortex and the corpus callosum.

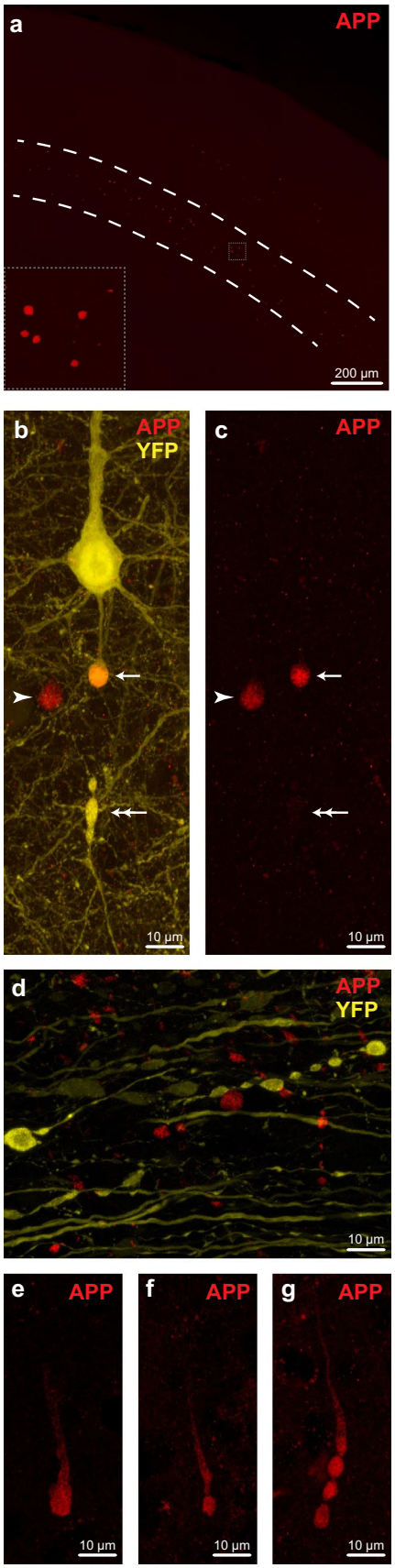

Fig. 6 TBI-induced APP accumulations display diverse morphologies which differ in their spatio-temporal distributions and extent of co-localization with YFP. **a** Large APP^+ bulbs were typically not randomly distributed across the cortex, but rather congregated in a band-like pattern, corresponding to cortical Layer V. **b**, **c** YFP^+APP^+ proximal bulbs were typically found close to their cell bodies of origin (*arrow*). In a few cases an axonal segment was located distal to the proximal bulb, with an orientation suggesting that they originated from the same axon. Unlike the proximal bulbs these distal axonal segments were APP^- (*double arrow*). Since only a subset of neurons express YFP there were also numerous YFP^-APP^+ bulbs (*arrowhead*). **d** The corpus callosum at 24 h post-injury contained numerous YFP^+ and APP^+ bulbs. Bulbs with dual markers, on the other hand, were not found, and if YFP and APP co-localized in the XY-plane they were always found to segregate in the Z-plane. **e** At 24 h post-injury the large, almost spherical, bulbs were very rare, although club-shaped bulbs were commonly found in the cortex. **f** At this time point there were also several cases within the cortex of what appeared to be a single bulb linked to a swollen axonal segment. **g** Axonal segments connected to multiple bulbs were also found in the cortical region 24 h post-injury, although these were very rare

Quantitation of APP labeling

To quantitatively determine the presence or absence of co-localization between APP and YFP a pixel-by-pixel analysis was performed (Fig. 7a). Sham-injured animals typically did not have any APP^+ bulbs and as expected displayed negligible levels of co-localization. Compared to sham-injured animals the cortical region from brain-injured animals had a substantially higher amount of co-localized positive pixels, particularly at 3 h, but also at 24 h, post-injury. The callosal region, on the other hand, displayed low levels of co-localization at both time points. The absence of co-localization was especially striking at 24 h post-injury, a time point at which the callosal region contained large numbers of both YFP^+ and APP^+ bulbs. The extent of co-labeling between YFP and APP was comparable in WT and KO mice and the results shown are a combination of both genotypes.

Only six APP^+ bulbs were found in the sham-injured mice and all of these were small and barely above the detection threshold, in stark contrast to the 1292 APP^+ bulbs found in brain-injured mice. Due to the scarcity of APP^+ bulbs in the sham-injured mice they were excluded from further analysis.

APP^+ bulb size did not follow a normal distribution but differed significantly (KS; $^{***}p < 0.001$) between Layer V of the cortex and the region encompassing the corpus callosum and deep cortical layers (Fig. 7b). Inspection of the distribution of the APP^+ bulbs revealed that those with a diameter of more than 4 µm were virtually absent in the corpus callosum and deep cortical gray, although frequently found in Layer V of the cortex. The scarcity of large APP^+ bulbs in the callosal region was similar in both WT and KO

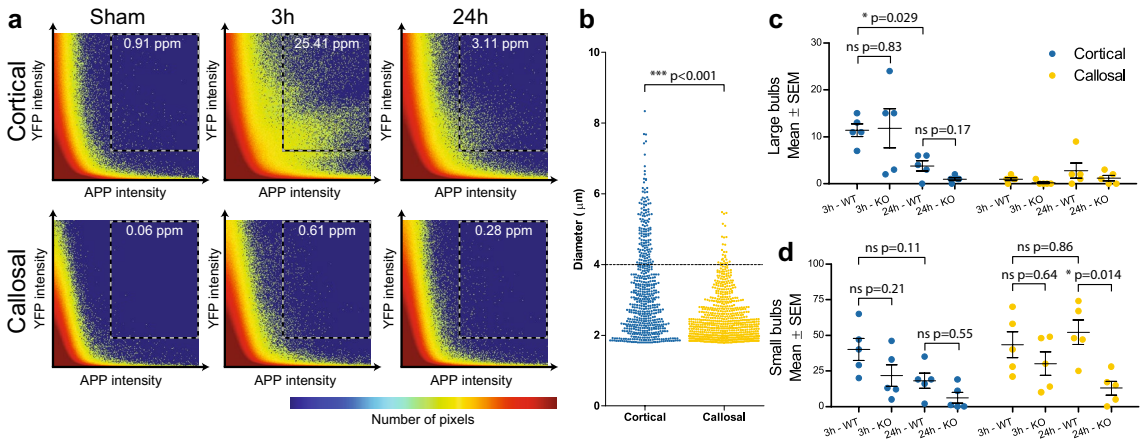

Fig. 7 Quantitation of APP$^+$ bulbs and their co-localization with YFP. **a** Visualization of YFP–APP co-localization and the fraction of co-localized pixels in parts per million (ppm). Note the clear increase in co-localization compared to sham-injury in the cortical region, particularly at 3 h post-injury. The low levels of co-localization in the callosal region is also noteworthy, given the presence of large number of small APP$^+$ bulbs as well as YFP$^+$ distal bulbs and varicosities in this region. **b** The distribution of APP$^+$ bulb size differs significantly between the cortical and callosal region. APP$^+$ bulbs with a diameter of more than 4 μm were numerous in the cortical region, although seldom found within the corpus callosum. **c** The number of large (diameter ≥4 μm) APP$^+$ bulbs in the cortical region was significantly reduced over time but not affected by CypD knock-out. **d** Small (diameter <4 μm) APP$^+$ bulbs were numerous in both the cortical and callosal regions, at 3 h as well as 24 h post-injury. The small callosal APP$^+$ bulbs were, however, substantially and significantly reduced by CypD knock-out

mice and the distribution is a combination of both genotypes. Both the pattern of co-labeling with YFP and the scarcity of large swellings in the corpus callosum indicates that the APP$^+$ bulbs consist of two distinct populations. Based on this the APP$^+$ bulbs were divided into large bulbs (diameter ≥4 μm) and small bulbs (diameter <4 μm), and analyzed separately.

The number of large APP$^+$ bulbs were non-normally distributed and differed between groups in the cortex (KW; $^{**}p = 0.0082$) but not in the callosal region (KW; ns $p = 0.24$) and the large callosal APP$^+$ bulbs were therefore not analyzed further. The number of large cortical APP$^+$ bulbs in WT mice was significantly reduced over time (BH; $^{*}p = 0.029$), but not by the CypD knock-out at neither 3 h, nor 24 h, post-injury (Fig. 7c). This is consistent with the results from the YFP$^+$ proximal bulbs, which by a qualitative assessment represent a subset of the large APP$^+$ cortical bulbs.

The small APP$^+$ bulbs followed a normal distribution with significant differences between groups in both the cortical (ANOVA; $^{*}p = 0.013$) and callosal region (ANOVA; $^{*}p = 0.016$). Pairwise comparisons did not reveal any significant differences in the numbers of small cortical APP$^+$ bulbs among the brain-injured groups. Similarly, the number of small callosal APP$^+$ bulbs was not significantly changed over time, but rather remained at almost identical levels. CypD knock-out did, however, result in an almost threefold, significant (TU; $^{*}p = 0.014$), reduction in the number of small callosal APP$^+$ bulbs at 24 h post-injury (Fig. 7d).

Ultrastructural analysis

The findings described above were readily confirmed in YFP$^+$ neurons and their axons using EM. The proximal bulbs were found to be unmyelinated and could typically be traced back to their cell bodies of origin. Even though the proximal bulbs were disconnected from the downstream axonal segment, they appeared morphologically intact, consistent with previous descriptions [24]. Comparably, the distal bulbs were found to be encompassed by a thinned myelin sheath and, although they revealed progressive change from 3 to 24 h they also remained intact. The use of the YFP immunolabeling also readily demonstrated distal bulb and varicosity formation (Fig. 8a). Unfortunately, the visualization of YFP$^+$ neurons and axons at the EM level proved less than optimal since the electron dense reaction product frequently obscured intra-axonal structural details, indicating that immunogold labeling may be preferable in future studies.

In this regard, the APP immunoreactive profiles provided considerably more information and detail. Antibodies to APP confirmed that the proximal bulbs were laden with APP, found within tubular and vesicular profiles of smooth endoplasmic reticulum. Embedded within these tubulovesicular profiles at 3 h post-injury were scattered intact mitochondria (Fig. 8b, c) and these organelles sometimes capped a disorganized cytoskeletal core. In these same preparations, distal, disconnected bulbs could be easily identified as they lacked any evidence of APP immunoreactivity and were always encompassed by a thinned myelin sheath (Fig. 8d). At 3 h

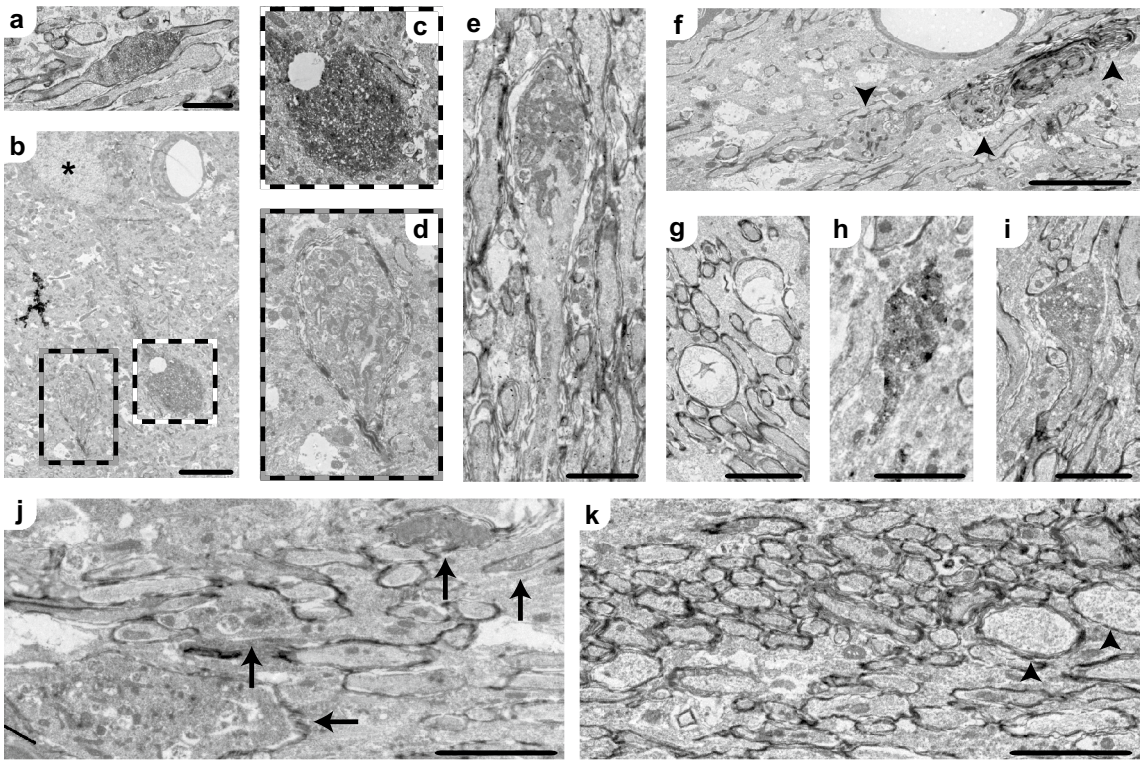

Fig. 8 Electron micrographs illustrating key features of injury-induced reactive axonal changes in WT (**a**–**j**) and KO (**k**) mice. **a** YFP expression clearly details distal bulb and varicosity formation. **b**–**d** Using antibodies to APP, a proximal bulb (*black*/*white* grid) can be seen in continuity with its cell body of origin (*asterisk*), while a distal bulb (*black*/*gray* grid) can also be identified at 3 h post-injury. Note that the proximal bulb (**c**) is not invested by a myelin sheath and contains a dense APP reaction product, while the distal bulb (**d**) is encompassed by a thinned myelin sheath and laden with organelles. **e** At 24 h post-injury distal bulbs typically displayed progressive expansion and WD. At 3 h post-injury, varicosity formation (**f**) can also be easily observed (*arrow heads*), as well as vacuolization of distal bulbs (**g**), both consistent with WD. At 3 h post-injury, APP immunoreactivity was detected in small bulbs within the corpus callosum. Note that these bulbs can originate from both unmyelinated (**h**) and myelinated (**i**) axons. At 24 h post-injury there was a striking difference between WT (**j**) and KO (**k**) mice. Note that the morphological signs of WD are extensive in WT tissue (*arrows*), but limited in the KO tissue (*arrow heads*). *Scale bar* 5 µm in B, F and 2 µm in all other micrographs

post-injury, the distal bulbs again revealed aggregations of tubulovesicular profiles with embedded mitochondria, which also could be found together with dense core vesicles and double membrane-bound vesicles (Fig. 8d). In addition to these changes consistent with Wallerian degeneration (WD), other distal bulbs manifested large vacuolated profiles (Fig. 8g), also consistent with previous descriptions of WD. At 3 h post-injury, distal bulb formation occurred in concert with varicosity development in the deeper cortical layers and corpus callosum. The multi-lobulated varicosities were encompassed by a thinned myelin sheath and contained vesicles devoid of APP as well as various electron dense inclusions (Fig. 8f). At 24 h post-injury the distal bulbs showed continued maturation with the accumulation of larger pools of tubulovesicular profiles, dense core vesicles and damaged mitochondria, which capped an expanded core of disorganized cytoskeletal constituents, again consistent with WD (Fig. 8e, j).

APP immunohistochemistry also revealed the presence of small APP^+ axonal bulbs within the corpus callosum (Fig. 8h, i). Consistent with the larger proximal bulbs these swellings contained APP^+ positive tubulovesicular profiles. Interestingly, even though these bulbs were devoid of a myelin sheath they originated from both myelinated (Fig. 8i) and unmyelinated (Fig. 8h) axons.

Lastly, EM allowed for a qualitative comparison of the structural changes ongoing in WT versus KO mice. Specifically, the WT mice typically revealed extensive pathology consistent with WD (Fig. 8j), while KO mice consistently revealed considerably improved tissue preservation (Fig. 8k), consistent with an attenuation of WD within the assessed post-injury time points.

Discussion

In the current communication we describe several distinct morphologies of injured axons (Table 1) and provide compelling evidence that some of these morphologies represent

Table 1 Characteristics of identified pathological axonal phenotypes

Phenotype	Description
Proximal bulbs	A single YFP$^+$ bulb still in continuity with its proximal, but not distal, axonal segment. Primarily found in the axon initial segment, always labeled with APP and were not reduced by CypD KO. Figures 2b, c, 6b and 8b,c
Varicosities (YFP$^+$)	A YFP$^+$ axon containing multiple bulbs. Found in both cortex and corpus callosum, did not label with APP but were reduced by CypD KO. Hypothesized to be present in axons undergoing Wallerian degeneration. Figures 2e–g, 6d and 8f
Distal bulbs	A single YFP$^+$ bulb disconnected from its proximal, but not distal, axonal segment. Share several characteristics with the YFP$^+$ varicosities and hypothesized to be part of the same underlying pathology. Figures 2d, g and 8b–e
Large APP$^+$ bulbs	A single APP$^+$ bulb with diameter ≥4 μm. Primarily found in cortical Layer V and were not reduced by CypD KO. Hypothesized to be present in the axon initial segment of Layer V pyramidal neurons. Figures 6a–c and 8b–c
Small APP$^+$ bulbs	A single APP$^+$ bulb with diameter <4 μm. Found in both the cortex and corpus callosum and were reduced by CypD KO at 24 h post-injury in the corpus callosum. Figures 6d and 8h–i
APP$^+$ clubs	Club-shaped APP accumulations found in cortical Layer V at 24 h post-injury. Figure 6e
APP$^+$ axo-bulbs	An APP accumulation connected to an APP$^+$ axonal profile. Found in cortical Layer V at 24 h post-injury. Figure 6f
Varicosities (APP$^+$)	Multiple connected APP$^+$ bulbs. Found in Layer V of the cortex 24 h post-injury at very low frequency. Hypothesized to be distinct from the YFP$^+$ varicosities based on APP content and spatial distribution. Figure 6g
Undulations	An axon with an undulating trajectory. Found in both sham- and brain-injured animals. Hypothesized to be a tissue preparation artifact. Figures 1, 2a, g

different stages of an evolving pathology, while others may occur in different axonal compartments or populations. The importance of this observation is illustrated by the effect of mitochondrial protection, which reduced the number of some, but not all, pathological axonal morphologies.

An example of pathophysiological progression within individual axons is the manner in which the proximal bulbs relate to the distal bulbs and varicosities. Our results demonstrate that distal bulbs and varicosities are two components of the same underlying pathology, and that they occur in axons undergoing WD induced by the axotomy at the site of the proximal bulb. This is supported by several independent observations, including the spatio-temporal distribution, the pattern of APP labeling and the ultrastructural findings. This interpretation is also supported by recent observations made following crush and/or transection of the optic nerve and spinal cord performed to induce WD [6]. These models resulted in formation of axonal bulbs with a spatio-temporal distribution similar to that observed in the current study, with the caveat that the temporal progression was somewhat slower in their models, perhaps reflecting differences between traumatic brain injury and transection paradigms. The molecular mechanism leading to this type of bulb formation is currently unknown, but our detailed description which demonstrates that individual bulbs typically are inter-connected, that they follow a Poisson distribution and that this distribution remains consistent over time, may be of utility in future studies in this area.

Our proposal that TBI-induced varicosities form in axons undergoing WD departs for current theories which suggest that varicosities are caused by mechanical damage at their site of formation. Specifically, Smith et al. [43] suggest a sequence of events where TBI induces undulation formation, microtubule breakage and partial interruption of axonal transport, which ultimately leads to varicosity formation. This hypothesis is, however, based on observations of thin unmyelinated axons evaluated in an in vitro model of axonal injury, which potentially differs from the in vivo situation in the rodent and human brain. Although we did see undulations in our model, these were present in both sham- and brain-injured animals. Undulations have previously been found in diseases and disease models devoid of mechanical forces [16, 26], further, it has also been convincingly demonstrated that undulating trajectories of neuronal processes can be induced by tissue processing [33], and we believe this to be the case in our study as well.

Varicosities with a morphology comparable to that found in the current study have also been described in multiple sclerosis and experimental autoimmune encephalitis (EAE), and have been suggested to be a new form of neuronal damage, termed focal axonal degeneration, caused by immune cells [35]. We have previously reported that axonal bulbs can occur as early as 15 min after injury in the cFPI model [23]. This rapid progression is not consistent with the temporal framework for microglia activation or macrophage infiltration, but rather points to an axon intrinsic pathway for bulb formation. Varicosity formation has also been observed following optic nerve transection performed ex vivo [6], which precludes immune cell involvement.

In this context it is also important to note that although the vast majority of varicosities found in this study lacked APP, we did find isolated cases of APP$^+$ varicosities. The scarcity of this phenotype precluded an evaluation of the mechanism of formation, but the presence of multiple phenotypes indicates that varicosities can be induced in at least two independent ways. Since the varicosities found in TBI patients

are APP$^+$ [43], they are more likely to be related to this study's less common finding of APP$^+$ varicosities, potentially associated with proximal axonal segments, than to the YFP$^+$ varicosities present in axons undergoing WD. This interpretation is further supported by our observation that APP labeling is limited to bulbs proximal to disconnection, which confirms our previous observations [23]. Beirowski et al. [6] did, however, note APP labeling in axonal segments undergoing WD, a discrepancy possibly caused by their use of an antibody targeting the N-terminus of APP, while we relied on a C-terminus targeting antibody. Our results thus demonstrate that C-APP labeling within YFP expressing neurons is restricted to bulbs located proximal to axotomies. Further studies are, however, required to precisely determine the extent of N-APP labeling and the spatial relationship between axotomies and callosal APP$^+$ bulbs.

Another important observation is the differential APP labeling pattern, where Layer V contained larger APP$^+$ bulbs which sometimes co-localized with YFP, while the APP$^+$ bulbs in the corpus callosum were smaller and never co-localized with YFP. The large APP$^+$ cortical bulbs are most likely located proximal to axotomy based on the co-localization with YFP seen in this study, as well as in previous reports [23]. The exact identity of the APP$^+$ callosal bulbs, on the other hand, is at present unknown, and although smaller in size than the proximal bulbs, they were morphologically similar to them, an observation most convincingly seen using EM. Specifically, ultrastructural analysis revealed that these bulbs contained APP$^+$ vesicles and were either encompassed by, or devoid of, a myelin sheath, and typically lacked morphological signs of WD. A potential caveat is that the absence of a myelin sheet at the bulb does not confirm that the axon was unmyelinated, since a lack of myelin may be caused by demyelination as well. Further, these APP$^+$ callosal bulbs were never found in YFP$^+$ axons, indicating that they most likely originated in an axonal population that did not include Layer V pyramidal neurons. It is also possible that the difference between Layer V and the corpus callosum reflects a differential response to trauma between different axonal compartments, such as the AIS and the nodes of Ranvier. Distinct populations of APP$^+$ axonal bulbs distinguishable by size have previously been reported in the brain stem [42], indicating that this is not an isolated phenomenon, but rather a finding that requires further investigations. The presence of neurofilament compaction adds further complexity to the axon injury pathology. This axonal morphology has previously been reported to occur in an axonal population separate from APP-containing axons, indicating the presence of an additional molecular mechanism leading to post-injury axonal pathology.

In addition to the detailed description of pathological phenotypes induced by TBI, we also attempted to reduce the detrimental consequences of mechanical axonal damage. Since axonal injury consistently has been associated with calcium influx, protease activation, and mitochondrial swelling [11], we hypothesized that opening of the mPTP and the ensuing calcium dysregulation is a potential therapeutic target for traumatic axonal injury. This is further supported by the effect of pharmacological inhibition of mPTP opening in rodent models, where Cyclosporin A treatment reduced axonal injury and NIM811 improved functional outcome [10, 34, 36, 39]. The structure of the mPTP has recently been elucidated and it is now firmly established that CypD is a regulatory, non-obligatory, component, whose absence reduces the likelihood of pore opening [1, 8, 9, 21]. In line with previous observations that Cyclosporin A reduces axonal injury in the brain stem [10, 36], we found that CypD knock-out reduced the numbers of small APP$^+$ callosal bulbs at 24 h post-injury, further supporting a detrimental role of mPTP opening in white matter tract axonal injury. Contrary to our expectations we were, however, unable to find any statistical evidence for reduced axonal injury in terms of neither YFP$^+$ proximal bulbs nor large cortical APP$^+$ bulbs. Based on our previous report these types of bulbs are mainly located within the AIS [23], an axonal compartment which differs substantially from the rest of the axon. These results thus strongly suggest that the pathobiology leading to bulb formation within the AIS differs from that of other axonal compartments.

The YFP$^+$ distal bulbs and varicosities were also reduced by CypD knock-out, and since these profiles are associated with disconnected, degenerating, axonal segments, this has important implications not only for TBI research, but also for the understanding of WD. It has recently been demonstrated that the spontaneous mutation slow Wallerian degeneration (Wld^S) increases mitochondrial calcium buffering capacity [2], and that CypD knock-out reduces WD in vitro and ex vivo [4]. However, despite these findings it has still been suggested that the role of mitochondria requires further clarification [13]. Therefore, in addition to the detailed morphological description of degenerating axons, we here present in vivo observations which further support a role for mitochondrial permeability transition as a key step in the execution of WD.

To conclude, our results provide several important insights into the axonal injury pathobiology. Firstly, the relationship between the YFP$^+$ proximal bulbs and varicosities demonstrates that axonal bulb formation can occur both before and after axotomy within the same axon. While we demonstrate that C-terminus APP specifically labels bulbs proximal to axotomy, there is a need to identify and validate specific molecular markers of the degenerating axonal segment. Secondly, we provide in vivo evidence for the importance of mPTP opening in WD as well as a detailed morphological description of degenerating axons.

Lastly, we provide further support for the importance of mPTP opening in white matter tract axonal injury while, contrary to our expectations, CypD knock-out did not reduce pathology within the AIS. This points to a difference in the pathobiology between axonal compartments, and a better understanding of this discrepancy may lead to the identification of novel treatment targets for axonal injury. In all, these results clearly illustrate the complexity of axonal injury and the need to consider the heterogeneity of the pathobiological process.

Acknowledgments The authors thank Carol Davis, Susan Walker and Jesse Sims for invaluable technical assistance, Scott Henderson and Frances White for sharing their expertise in confocal microscopy, Audrey Lafrenaye, Vishal Patel and Michal Vascak for scientific discussions and comments on this manuscript as well as Michael Forte and Paolo Bernardi for generating and providing the CypD KO mice. This work was funded by NIH grants NS077675 and NS047463.

Conflict of interest The authors declare that they have no conflict of interest.

Ethical approval All applicable international, national, and/or institutional guidelines for the care and use of animals were followed.

References

1. Alavian KN, Beutner G, Lazrove E, Sacchetti S, Park HA, Licznerski P et al (2014) An uncoupling channel within the c-subunit ring of the F1FO ATP synthase is the mitochondrial permeability transition pore. Proc Natl Acad Sci 111:10580–10585
2. Avery MA, Rooney TM, Pandya JD, Wishart TM, Gillingwater TH, Geddes JW et al (2012) WldS prevents axon degeneration through increased mitochondrial flux and enhanced mitochondrial Ca2+ buffering. Curr Biol 22:596–600
3. Baines CP, Kaiser RA, Purcell NH, Blair NS, Osinska H, Hambleton MA et al (2005) Loss of cyclophilin D reveals a critical role for mitochondrial permeability transition in cell death. Nature 434:658–662
4. Barrientos SA, Martinez NW, Yoo S, Jara JS, Zamorano S, Hetz C et al (2011) Axonal degeneration is mediated by the mitochondrial permeability transition pore. J Neurosci 31:966–978
5. Basso E, Fante L, Fowlkes J, Petronilli V, Forte MA, Bernardi P (2005) Properties of the permeability transition pore in mitochondria devoid of Cyclophilin D. J Biol Chem 280:18558–18561
6. Beirowski B, Nogradi A, Babetto E, Garcia-Alias G, Coleman MP (2010) Mechanisms of axonal spheroid formation in central nervous system Wallerian degeneration. J Neuropathol Exp Neurol 69:455–472
7. Benjamini Y, Hochberg Y (1995) Controlling the false discovery rate—a practical and powerful approach to multiple testing. J Roy Stat Soc Ser B Methodol 57:289–300
8. Bernardi P (2013) The mitochondrial permeability transition pore: a mystery solved? Front Physiol 4:95
9. Bonora M, Bononi A, De Marchi E, Giorgi C, Lebiedzinska M, Marchi S et al (2013) Role of the c subunit of the FO ATP synthase in mitochondrial permeability transition. Cell Cycle 12:674–683
10. Buki A, Okonkwo DO, Povlishock JT (1999) Postinjury cyclosporin A administration limits axonal damage and disconnection in traumatic brain injury. J Neurotrauma 16:511–521
11. Buki A, Povlishock JT (2006) All roads lead to disconnection? Traumatic axonal injury revisited. Acta Neurochir (Wien) 148:181–193 (discussion 193–184)
12. Cesarovic N, Nicholls F, Rettich A, Kronen P, Hassig M, Jirkof P et al (2010) Isoflurane and sevoflurane provide equally effective anaesthesia in laboratory mice. Lab Anim 44:329–336
13. Conforti L, Gilley J, Coleman MP (2014) Wallerian degeneration: an emerging axon death pathway linking injury and disease. Nat Rev Neurosci 15:394–409
14. Dikranian K, Cohen R, Mac Donald C, Pan Y, Brakefield D, Bayly P et al (2008) Mild traumatic brain injury to the infant mouse causes robust white matter axonal degeneration which precedes apoptotic death of cortical and thalamic neurons. Exp Neurol 211:551–560
15. Du H, Guo L, Fang F, Chen D, Sosunov AA, McKhann GM et al (2008) Cyclophilin D deficiency attenuates mitochondrial and neuronal perturbation and ameliorates learning and memory in Alzheimer's disease. Nat Med 14:1097–1105
16. Dziedzic T, Metz I, Dallenga T, Konig FB, Muller S, Stadelmann C et al (2010) Wallerian degeneration: a major component of early axonal pathology in multiple sclerosis. Brain Pathol 20:976–985
17. English AW, Meador W, Carrasco DI (2005) Neurotrophin-4/5 is required for the early growth of regenerating axons in peripheral nerves. Eur J Neurosci 21:2624–2634
18. Ewald AJ, Werb Z, Egeblad M (2011) Monitoring of vital signs for long-term survival of mice under anesthesia. Cold Spring Harb Protoc. pdb prot5563
19. Feng G, Mellor RH, Bernstein M, Keller-Peck C, Nguyen QT, Wallace M et al (2000) Imaging neuronal subsets in transgenic mice expressing multiple spectral variants of GFP. Neuron 28:41–51
20. Forte M, Gold BG, Marracci G, Chaudhary P, Basso E, Johnsen D et al (2007) Cyclophilin D inactivation protects axons in experimental autoimmune encephalomyelitis, an animal model of multiple sclerosis. Proc Natl Acad Sci 104:7558–7563
21. Giorgio V, von Stockum S, Antoniel M, Fabbro A, Fogolari F, Forte M et al (2013) Dimers of mitochondrial ATP synthase form the permeability transition pore. Proc Natl Acad Sci 110:5887–5892
22. Goldstein LE, Fisher AM, Tagge CA, Zhang XL, Velisek L, Sullivan JA et al (2012) Chronic traumatic encephalopathy in blast-exposed military veterans and a blast neurotrauma mouse model. Sci Transl Med 4:134ra160
23. Greer JE, Hanell A, McGinn MJ, Povlishock JT (2013) Mild traumatic brain injury in the mouse induces axotomy primarily within the axon initial segment. Acta Neuropathol 126:59–74
24. Greer JE, McGinn MJ, Povlishock JT (2011) Diffuse traumatic axonal injury in the mouse induces atrophy, c-Jun activation, and axonal outgrowth in the axotomized neuronal population. J Neurosci 31:5089–5105
25. Hayat MJ, Higgins M (2014) Understanding poisson regression. J Nurs Educ 53:207–215
26. Haynes RL, Billiards SS, Borenstein NS, Volpe JJ, Kinney HC (2008) Diffuse axonal injury in periventricular leukomalacia as determined by apoptotic marker fractin. Pediatr Res 63:656–661
27. Hulkower MB, Poliak DB, Rosenbaum SB, Zimmerman ME, Lipton ML (2013) A decade of DTI in traumatic brain injury: 10 years and 100 articles later. AJNR Am J Neuroradiol 34:2064–2074
28. Ikonomovic MD, Uryu K, Abrahamson EE, Ciallella JR, Trojanowski JQ, Lee VM et al (2004) Alzheimer's pathology in human temporal cortex surgically excised after severe brain injury. Exp Neurol 190:192–203
29. Johnson VE, Stewart W, Smith DH (2013) Axonal pathology in traumatic brain injury. Exp Neurol 246:35–43

30. Kinnunen KM, Greenwood R, Powell JH, Leech R, Hawkins PC, Bonnelle V et al (2011) White matter damage and cognitive impairment after traumatic brain injury. Brain 134:449–463
31. Lafrenaye AD, McGinn MJ, Povlishock JT (2012) Increased intracranial pressure after diffuse traumatic brain injury exacerbates neuronal somatic membrane poration but not axonal injury: evidence for primary intracranial pressure-induced neuronal perturbation. J Cereb Blood Flow Metab 32:1919–1932
32. Luvisetto S, Basso E, Petronilli V, Bernardi P, Forte M (2008) Enhancement of anxiety, facilitation of avoidance behavior, and occurrence of adult-onset obesity in mice lacking mitochondrial cyclophilin D. Neuroscience 155:585–596
33. Marx M, Gunter RH, Hucko W, Radnikow G, Feldmeyer D (2012) Improved biocytin labeling and neuronal 3D reconstruction. Nat Protoc 7:394–407
34. Mbye LH, Singh IN, Carrico KM, Saatman KE, Hall ED (2009) Comparative neuroprotective effects of cyclosporin A and NIM811, a nonimmunosuppressive cyclosporin A analog, following traumatic brain injury. J Cereb Blood Flow Metab 29:87–97
35. Nikic I, Merkler D, Sorbara C, Brinkoetter M, Kreutzfeldt M, Bareyre FM et al (2011) A reversible form of axon damage in experimental autoimmune encephalomyelitis and multiple sclerosis. Nat Med 17:495–499
36. Okonkwo DO, Povlishock JT (1999) An intrathecal bolus of cyclosporin A before injury preserves mitochondrial integrity and attenuates axonal disruption in traumatic brain injury. J Cereb Blood Flow Metab 19:443–451
37. Palma E, Tiepolo T, Angelin A, Sabatelli P, Maraldi NM, Basso E et al (2009) Genetic ablation of cyclophilin D rescues mitochondrial defects and prevents muscle apoptosis in collagen VI myopathic mice. Hum Mol Genet 18:2024–2031
38. Povlishock JT, Katz DI (2005) Update of neuropathology and neurological recovery after traumatic brain injury. J Head Trauma Rehabil 20:76–94
39. Readnower RD, Pandya JD, McEwen ML, Pauly JR, Springer JE, Sullivan PG (2011) Post-injury administration of the mitochondrial permeability transition pore inhibitor, NIM811, is neuroprotective and improves cognition after traumatic brain injury in rats. J Neurotrauma 28:1845–1853
40. Sherriff FE, Bridges LR, Sivaloganathan S (1994) Early detection of axonal injury after human head trauma using immunocytochemistry for beta-amyloid precursor protein. Acta Neuropathol 87:55–62
41. Stone JR, Okonkwo DO, Dialo AO, Rubin DG, Mutlu LK, Povlishock JT et al (2004) Impaired axonal transport and altered axolemmal permeability occur in distinct populations of damaged axons following traumatic brain injury. Exp Neurol 190:59–69
42. Stone JR, Walker SA, Povlishock JT (1999) The visualization of a new class of traumatically injured axons through the use of a modified method of microwave antigen retrieval. Acta Neuropathol 97:335–345
43. Tang-Schomer MD, Johnson VE, Baas PW, Stewart W, Smith DH (2012) Partial interruption of axonal transport due to microtubule breakage accounts for the formation of periodic varicosities after traumatic axonal injury. Exp Neurol 233:364–372
44. Tang-Schomer MD, Patel AR, Baas PW, Smith DH (2010) Mechanical breaking of microtubules in axons during dynamic stretch injury underlies delayed elasticity, microtubule disassembly, and axon degeneration. FASEB J 24:1401–1410